Research Square

Preprints are preliminary reports that have not undergone peer review.
They should not be considered conclusive, used to inform clinical practice,
or referenced by the media as validated information.

Hepatocyte mitochondrial DNA regulates the formation of extracellular traps by kidney macrophages: a potential factor in liver-kidney crosstalk in TCE-sensitized mice

Xueqian Jia
Anhui Medical University School of Public Health
Xuan Fan
Anhui Medical University School of Public Health
Chenghuan Wan
Anhui Medical University School of Public Health
Zijun Li
Anhui Medical University School of Public Health
Luqing Pan
Anhui Medical University School of Public Health
Hui Wang
Department of Prevention and Health Care, Chaohu Hospital of Anhui Medical University, Hefei, Anhui Province, China
Jiaxiang Zhang
jiaxiang5337@ahmu.edu.cn

Anhui Medical University School of Public Health

Research Article

Keywords: Trichloroethylene, hepatocyte mtDNA, macrophages, M1polarization, extracellular traps

Posted Date: August 3rd, 2026

DOI: https://doi.org/10.21203/rs.3.rs-9963869/v1

License: This work is licensed under a Creative Commons Attribution 4.0 International License.
Read Full License

Additional Declarations: No competing interests reported.

Abstract

Trichloroethylene (TCE) is a common industrial organic solvent. Exposure to TCE can induce occupational medicamentosa-like dermatitis (OMDT), which is frequently accompanied by liver and kidney injury. During the organ damage caused by TCE, mtDNA is a key molecule that mediates the interaction between the liver and the kidney. Our previous research has shown that mitochondrial DNA (mtDNA) released from hepatocytes damage under TCE sensitization can cause damage to renal tubular epithelial cells. However, the specific mechanism remains unclear. To this end, we established a TCE percutaneous sensitization mouse model. We found that in the TCE sensitization positive group, liver damage was strongly correlated with kidney damage. The Stimulator of Interferon Genes (STING) pathway in renal macrophages was activated, and the macrophages underwent M1 polarization accompanied by the formation of macrophage extracellular traps (METs). To further confirm the role of hepatocyte mtDNA, we extracted the mtDNA from the hepatocytes of TCE sensitization positive mice and injected it into normal mice. We found that the STING pathway in the kidney of the injection group was activated, and the macrophages also underwent M1 polarization. This phenomenon was significantly alleviated after intervention with the STING inhibitor C-176. We also confirmed this in vitro using RAW264.7 with hepatocyte mtDNA treatment. In summary, our work demonstrated that hepatocyte mtDNA can activate the STING pathway in renal macrophages, thereby causing M1 polarization of macrophages and the formation of METs. C-176 can alleviate this phenomenon.

1. Introduction

Trichlorojethylene (TCE) is a chlorinated olefin compound (Ma et al., 2022), as a volatile industrial organic solvent, it is commonly used in metal cleaning, extraction solvents, and other industrial field (Su et al., 2023). Some reports have shown that workers exposed to TCE may develop occupational dermatitis-like drug eruption caused by trichloroethylene (OMDT). In 2025, the diagnostic criteria for this disease were further revised and implemented (Nakajima et al., 2022). The main clinical manifestations are acute dermatitis, mostly exfoliative dermatitis. In addition to skin lesions, OMDT is often accompanied by liver injury, kidney injury, and nervous system damage. Clinical observations have shown that liver injury in patients may be followed by secondary kidney injury, but the underlying cause remains unclear. Previous studies have identified hepatocyte mitochondrial DNA (mtDNA) as a key factor mediating liver-kidney crosstalk. However, the mechanism of hepatocyte mtDNA mediates kidney injury has not yet been fully elucidated in TCE sensitization.

mtDNA is a double-stranded circular genome normally confined to the mitochondrial matrix. Under conditions of cellular stress or injury, mtDNA can be released into the extracellular circulation and function as a damage-associated molecular pattern (DAMP). Owing to its bacterial origin and unmethylated CpG motifs, extracellular mtDNA is recognized by pattern recognition receptors (PRRs) (Garg et al., 2023), such as Toll-like receptor 9 (TLR9), leading to macrophage activation and M1 polarization, which subsequently triggers the release of pro-inflammatory cytokines and contributes to inflammatory injury in distant organs (Zuo et al., 2024). Moreover, it can also cause calcium influx in

renal podocytes through the cGAS-STING pathway, leading to calcium imbalance and activating the SOCE pathway, stimulating podocytes to secrete inflammatory factors such as IL-6 and CXCL10, thereby aggravating glomerular filtration injury (Dong et al., 2025). Macrophages play an important role in the innate immune response. Previously, our research group found that hepatocyte mtDNA regulates the M1 polarization of macrophages by activating the TLR9 signaling pathway in liver macrophages (Gao et al., 2024). TCE sensitization is characterized by a systemic immune-mediated response in which macrophage activation plays a pivotal role. Although liver injury is a prominent feature of this condition, clinical observations indicate that kidney damage often occurs during disease progression. To investigate the molecular mechanisms underlying this phenomenon, we performed a proteomic analysis of kidney tissues. The results revealed a significant enrichment of differentially expressed proteins in the "Phagosome" pathway. As phagocytosis is a core function of macrophages (Russell et al., 2009),this finding serves as a robust indicator that renal macrophages are actively responding to TCE exposure.These findings raise the possibility that renal macrophages may serve as key effector cells in TCE-induced kidney injury (Gao et al., 2024). However, whether hepatocyte mtDNA participates in the activation of renal macrophages and the underlying mechanisms by which it contributes to kidney injury in the context of TCE sensitization remain to be elucidated.

Previous studies have confirmed that TCE can induce abnormal activation of macrophages (Gao et al., 2025). Our previous research also found that mtDNA of liver cells is a key effector molecule mediating the liver-kidney crosstalk under TCE sensitization, and it is also an important upstream basis for regulating macrophage activation (Gao et al., 2024). Current studies have clearly demonstrated that macrophages play a core regulatory role in the occurrence and development of immune-related kidney injury. Besides exerting classic anti-inflammatory and pro-inflammatory effects, macrophages can also be activated to form a network structure, namely macrophage extracellular trapping network (METs), which is similar to the structure of neutrophil extracellular trapping network (NETs). Macrophages can also release extracellular trapping networks (ETs) after being exposed to various pathogens and pro-inflammatory stimuli. This important immune phenomenon was first reported by Brinkmann et al. in 2004 and systematically described in neutrophil (Liu et al., 2025). It is a complex network structure composed of DNA and various active proteins. Its release is usually accompanied by cell lysis. Macrophages and neutrophils are both immune cells, and the nature of the stimulus can affect the formation pathway of METs (Conceição-Silva et al., 2021). Under physiological conditions, METs have the functions of capturing and killing pathogens and are an immune protection mechanism produced by macrophages, which can kill pathogenic microorganisms, regulate inflammatory responses, and maintain immune homeostasis (Rasmussen and Hawkins, 2022). However, under pathological conditions, studies have shown that METs are considered to be related to the occurrence and development of various diseases (Okubo et al., 2018). Some scholars have pointed out that macrophages in the inflammatory M1 phenotype are more likely to release METs, for example, M1-type macrophages induced by IFN-γand LPS will release METs, while M2-type macrophages induced by IL-4 do not release METs (Nakazawa et al., 2016; Rayner et al., 2018). In conclusion, the release of METs is a double-edged sword. Under pathological conditions, the released METs will further exacerbate the

inflammatory response. In this study, whether liver cell mtDNA triggers the formation of kidney METs and aggravates TCE-induced kidney injury, and the specific mechanism is currently unclear.

As a DNA receptor, cGAS can recognize both endogenous and exogenous double-stranded DNA, including viral DNA, bacterial DNA, genomic DNA and mitochondrial DNA, and synthesize the second messenger cGAMP (Wang et al., 2022). cGAMP binds to STING anchored on the endoplasmic reticulum. In a quiescent state, the STING molecule binds to the endoplasmic reticulum in a dimeric form. When activated by the cGAMP signal, the STING molecule transforms from a dimer to a tetramer, undergoes a spatial structural change, detaches from the endoplasmic reticulum and subsequently moves to the Golgi apparatus (Xian et al., 2022). The activated STING molecule activates its downstream IKKα/IKBα/NF-κB signaling pathway through a cascade reaction. After activation, the κB inhibitor kinase α (IKKα) can phosphorylate the nuclear factor -κB inhibitor (IKBα), allowing the nuclear factor -κB (NF-κB) to be released, resulting in the nuclear translocation of the nuclear transcription factor NF-κB, and subsequently triggering the transcription and release of inflammatory factors (Chen et al., 2023).

This study intends to deeply explore the specific molecular mechanisms of liver and secondary kidney injury during TCE sensitization, clarify whether mtDNA of liver cells can serve as a messenger molecule between cells, and through mediating the formation and polarization of METs in renal macrophages, participate in the secondary process of liver injury leading to kidney injury. We are hoping to provide new theoretical basis and potential intervention targets for the prevention and treatment of multi-organ damage in OMDT.

2. Methods

2.1. Chemicals and reagents

The antibodies and reagents used and their suppliers were as follows: TCE and Fuchs' Complete Adjuvant (FCA) were purchased from Sigma (St. Louis, MO, USA). Acetone and olive oil were purchased from Shanghai Chemical Reagent Company (Shanghai, China). mtDNA isolation kit was purchased from Abcam, mouse IL-6 and TNF-α ELISA kits were purchased from Jianglai Biotechnology, BUN, CRE, ALT, and AST detection kits were purchased from Nanjing Jiancheng Biotechnology Research Institute, and the STING inhibitor C-176 was purchased from Selleck. cGAS, F4/80, and NF-κB p65 were purchased from Santa Cruz, USA; STING was purchased from Wuhan Sanying; P-IKBα was purchased from Abmart; IKBα was purchased from Abclonal; NF-κB p-p65 was purchased from Immunity; MPO, iNOS, and P-IKKα were purchased from Selleck; CitH3 and PAD4 were purchased from Abcam; GAPDH and β-tubulin were purchased from Wuhan Servicebio.

2.2 Extraction of liver cells

After anesthetizing the mice, the chest cavity was opened and the portal vein and inferior vena cava were carefully separated. The needle was inserted parallel to the vessel into the portal vein and perfusion began. At the beginning of perfusion, the inferior vena cava of the mice should be cut immediately and

the flow rate adjusted. When there was no blood in the vessels, the perfusion tube was placed in the IV type collagenase for perfusion. The inferior vena cava was clamped with forceps to allow the enzyme solution to flow through the liver fully, enabling the liver to fully digest. After about 5 minutes, the perfusion was stopped. The gallbladder was carefully removed and the liver was cut and placed in a culture dish containing culture medium. The tissue was torn apart with forceps, the capsule was removed, and the cell suspension was filtered through a cell filter using a syringe and transferred to a 50 mLcentrifuge tube at 4℃. The centrifuge tube was centrifuged for 2 minutes at 54 g, washed twice with PBS, and the sediment was collected for subsequent experiments.

2.3 Mitochondrial DNA extraction

Collect cells by centrifugation at 600 g for 5 min and wash with PBS. Centrifuge for 5 min and resuspend pellet in cytosol extraction buffer. Incubate on ice for 10 min- homogenize in dounce tissue grinder. Centrifuge for 10 min at 700 g to pellet nuclei and intact cells. Transfer supernatant and centrifuge at 10,000 g for 30 min. Remove supernatant, resuspend pellet in cytosol extraction buffer and centrifuge at 10,000 g for 30 min. Resuspend pellet (mitochondria) and lyse in mitochondrial lysis buffer for 10 min Add enzyme mix and incubate for 60 min. Add ethanol and incubate for 10 min. Centrifuge for 5 min and retain pellet (mitochondrial DNA). The extracted mtDNA was subjected to purity and concentration testing before being injected into the tail vein.

2.4 Animal modeling and grouping

2.4.1 Establishment of TCE animal model

A total of 91 SPF female BALB/c mice aged 6 to 8 weeks were derived from the Experimental Animal Center of Anhui Medical University One day before the modeling, the hair in an area approximately 2×2 square centimeters on the back of the mice was removed, and the mice were then grouped: blank control group (n = 12), solvent control group 0 (n = 12, TCE-treated group (n = 35), and TCE + C-176 treated group (n = 32). On the first day of modeling, inject a mixture of 50 μL FCA and 50% TCE (TCE: olive oil: acetone = 5:2:3) composed of 100 μL into the subcutaneous area of the backs of each mouse for the first stimulation. On the 4th, 7th, and 9th days of modeling, apply 100 μL of 50% TCE to the backs of each mouse by skin application. On the 17th and 19th days of modeling, apply 100 μLof 30% TCE (TCE: olive oil: acetone = 3:2:5) to the backs of each mouse, and give the TCE + C-176 combined treatment group mice intraperitoneal injection of 10mg/kg C-176 (STING inhibitor) 2 hours before the 17th and 19th days of exposure. On the 20th day, score the skin reaction on the backs of the mice. A score of ≥ 1 indicates a positive sensitization, otherwise it is a positive sensitization. After scoring, euthanize the mice and collect the corresponding blood and urine.

2.4.2 An experiment on the mtDNA of liver cells in sensitized positive mice injected with TCE through the tail vein

A total of 30 SPF female BALB/c mice were randomly grouped after 1 week of adaptive feeding: solvent control group (n = 6), mtDNA injection group (n = 12), and mtDNA + C-176 treatment group (n = 12). On

the first and second days, mice in the mtDNA + C-176 treatment group were injected with the C-176 (10mg/kg), while the other two groups did not receive any treatment; on the third day, mice in the mtDNA tail vein injection group and the mtDNA + C-176 treatment group were injected with 5μg of purified mtDNA, and the solvent control group was given the same volume of normal saline; 24 hours later, all mice were anesthetized and samples were collected uniformly.

2.5 Proteome

Kidney tissues from both the TCE-positive and Blank control groups were subjected to proteomic sequencing. Tissue samples were homogenized in RIPA lysis buffer containing 1 mmol/L PMSF. Following homogenization, the lysates were centrifuged at 12,000×g for 10 minutes at 4°C to eliminate insoluble debris. Protein concentrations were then quantified using a BCA assay to ensure they met the standards required for proteomic analysis. For protein digestion, samples were incubated overnight at 37°C with 10 ng/mL trypsin in a 50 mM NH_4HCO_3 solution. The resulting peptides were desalted using SOLA™ SPE cartridges, vacuum-dried, and subsequently resuspended with the addition of iRT peptides at a ratio of 1:20.

Proteomic data acquisition was conducted by Shanghai OE Biotech Co., Ltd. (Shanghai, China). Data acquisition was performed by a Tims TOF Pro mass spectrometer (Thermo, Bruker) equipped with an Easyspray source (Thermo, USA). Peptide separation was achieved using a C18 column (15cm×75μm) on an EASY-nLC 1200 system (Thermo, USA) at a flow rate of 300 nL/min. The mobile phase gradient was programmed as follows: 5–22% B over 0–20 min, 22–37% B over 20–24 min, 37–80% B over 24–27 min, and maintained at 80% B from 27–30 min. Additional instrument parameters were set as follows: ion mobility range of 0.7–1.3 Vs/cm^2, collision energy range of 20–59 eV, and an MS/MS scan range of 100–1700 m/z.

2.6 ELISA analysis

Restore the serum and reagents in the kit to room temperature and prepare the standards. Add 50 μL of the detection buffer to each well, then add 10 μL of the standard and the sample. Add 50 μL of the detection antibody to each well, seal the plate, and shake at 500 revolutions per minute at room temperature for 1 hour. Discard the liquid and dry it. Add 300 μL of the washing solution to each well, wash 4 times. Add 100 μL of the horseradish peroxidase marker, replace the sealing membrane, and shake at 500 revolutions per minute at room temperature for 30 minutes. Repeat the washing. Add 100 μL of the color development substrate TMB to each well, incubate at room temperature for 5–30 minutes. After the standard clearly shows color, add 100 μL of the termination solution to each well. Measure the OD value at 450 nm within 30 minutes.

2.7 HE staining

The liver and kidney paraffin sections were baked at 100℃ for 20 minutes. While still hot, they were placed in 1, 2, and 3 of the xylene solutions for 10 minutes each for dewaxing. Then, they were placed in 100%, 90%, 70%, and 50% alcohol for 5 minutes each for dehydration. The sections were rinsed with

water for 5 minutes, washed with PBS for 3×5 minutes. After drying, 3 minutes of safranin staining solution was added, followed by 5 minutes of water rinsing. 1 minute of eosin staining solution was added, and 30 seconds of water rinsing were conducted. Under the microscope, the staining was observed. If the staining was poor, re-staining could be performed. After 5 minutes of water rinsing, the sections were dried at 60℃ for 20 minutes and sealed with neutral resin.

2.8 Immunohistochemistry analysis

The steps of baking, dewaxing, dehydration, etc. are the same as those in HE staining. The sections were treated with 40℃ cell permeation solution for 40 minutes, washed with PBS, heated and cooled repeatedly in a microwave oven in a citrate sodium solution to room temperature, then washed with PBS. 37℃ internal peroxidase was added and incubated for 20 minutes. Subsequently, the primary antibody was incubated at 4℃ overnight, followed by incubation with the secondary antibody and horseradish peroxidase working solution at 37℃, washed with PBS, and then stained with DAB under a microscope. The nuclei were stained with hematoxylin, dried, and mounted with neutral resin for microscopic examination.

2.9 Western blot analysis

The extracted primary hepatocytes and primary macrophages were lysed with RIPA lysis buffer containing 1% PMSF on ice. The cells were lysed and centrifuged at 1500 rpm for 15 minutes, followed by quantification with a BCA kit. The proteins obtained by lysis were separated on acrylamide gels, and the proteins separated on the acrylamide gels were transferred to polyvinylidene difluoride (PVDF) membranes. The transferred PVDF membrane was blocked with 5% skim milk for 2 hours. Afterwards, the sections were incubated overnight in a refrigerator at 4℃ with the primary antibody. The next day, after being washed three times with TBST, the membrane was blocked for 2 hours at room temperature with anti-mouse IgG or anti-rabbit IgG. Finally, the assay was performed with an enhanced chemiluminescence (ECL) assay kit. The results were processed with Image-Pro Plus software 6.0 (Media Cy bernetics, USA).

2.10 Data analysis

The data are presented as mean ± standard deviation. Quantitative analysis of Western blot bands was performed using ImageJ software. Student's t-test was used for comparison between the two groups, and one-way analysis of variance (ANOVA) combined with Tukey's post-hoc test was used for comparisons among multiple groups. $P < 0.05$ indicates a statistically significant difference.

3. Results

3.1 The sensitization rate of TCE-sensitized mice and the conditions of liver and kidney damage

On the 21st day of the modeling process, we conducted a scoring of the skin on the back of the mice. (Fig. 1a) Among them, the skin of the TCE sensitization negative group showed no response, while the severity of the skin of the TCE sensitization positive group mice could be classified from low to high as: scattered mild redness, moderate and diffuse redness and swelling, dense erythema and swelling. The sensitization rates of the TCE sensitization positive group and the TCE + C-176 sensitization positive group were respectively 34.3% and 37.5%.

To explore the liver and kidney injuries in TCE-sensitized mice, we found through HE staining that compared with the blank control group and the solvent control group, there was inflammatory cell infiltration of hepatocytes in the TCE-sensitized positive group(TCE+). (Fig. 1b) In addition, the results of transmission electron microscopy indicated that the mitochondrial structure of hepatocytes in the TCE+ group of mice was disordered, and the outer mitochondrial membrane disappeared. The above results indicate that mice in the TCE sensitization positive group have liver injury and damage to the mitochondria of hepatocyte. (Fig. 1c) The results of HE staining of the kidneys suggested that the kidneys were also damaged in TCE+ group mice. Interestingly, the addition of the STING inhibitor C-176 could alleviate this phenomenon. (Fig. 1d) The results of liver function indicators (ALT, AST) and renal function indicators (CRE, BUN) showed that compared with the blank control group and the solvent control group, the indicators in the TCE+ group significantly increased. (Fig. 1e) In previous studies, we confirmed a significant correlation between liver and kidney injury in OMDT patients. Therefore, we further analyzed the connection between liver and kidney injury indicators in TCE-sensitized mice. The results also indicated that there was a certain connection between liver and kidney damage in TCE-sensitized mice.

3.2 Macrophage activation and M1-type polarization

We performed a comprehensive proteomic analysis of kidney tissues from the TCE-positive group and the blank control group. Principal component analysis showed a clear separation between the two groups, indicating distinct proteomic profiles following TCE exposure (Fig. 2a). Using a cutoff of fold change ≥ 2.0 and $P < 0.05$, a total of 203 differentially expressed proteins were identified, including 133 upregulated and 70 downregulated proteins in the TCE-positive group compared with the blank control group (Fig. 2b). Kyoto Encyclopedia of Genes and Genomes enrichment analysis revealed that these differentially expressed proteins were significantly enriched in the phagosome pathway (Fig. 2c). Since phagocytosis is a key functional feature of activated macrophages, the enrichment of this pathway suggests that TCE exposure may be associated with macrophage activation and enhanced phagocytic activity in the kidney.We also investigated whether renal macrophages underwent activation and M1-type polarization. The immunohistochemical results showed that compared with the blank control group and the solvent control group, the renal macrophages in the TCE+ group were significantly activated, and the expression level of M1-type protein iNOS was significantly increased. C-176 could significantly alleviate macrophage activation and reduce the expression of iNOS (Fig. 2d).

3.3 Activation of the STING pathway in the kidneys of TCE-sensitized mice

As mentioned earlier, in the TCE sensitization positive group, both the liver and kidneys were damaged to varying degrees, and C-176 could alleviate kidney damage. Based on the results of further transcriptome analysis, changes in inflammatory and immune-related signaling pathways were shown. We verified the STING pathway and its downstream NF-κB inflammatory axis,we first detected the expression of STING protein through immunofluorescence experiments. The results showed that in TCE+ group, the macrophage marker protein F4/80 and STING were significantly co-localized (Fig. 3a). The western blotting experiment also further demonstrated that in the TCE+ group, the expression of STING and its downstream proteins significantly increased, and C-176 could significantly reduce the expression of downstream proteins (Fig. 3b). These results indicate that the STING pathway in renal macrophages is activated during the TCE sensitization process.

3.4 Generation of METs in the kidneys of TCE-sensitized mice

Based on the above results indicating that TCE can activate the STING/NF-κB inflammatory signaling pathway, we further evaluated whether TCE exposure induces the formation of NETs in the macrophage-related inflammatory microenvironment and the changes in their molecular markers.Some literature indicates that M1-polarized macrophages are more prone to METs (Nakazawa et al., 2016; Rayner et al., 2018). Therefore, we explored the expression of METs in macrophages through immunofluorescence experiments, and the results showed that compared with the solvent control group, the expression of citH3 in the TCE+ group was significantly increased, and it had a relatively obvious co-localization with F4/80 (Fig. 4a). The results of protein immunoblotting showed that compared with the blank control group, the solvent control group, and the TCE- group, the METs marker proteins citH3, PAD4, and MPO in the TCE+ group were significantly upregulated, but their expression levels decreased after adding C-176 (Fig. 4b). In summary, these results indicate that during the TCE sensitization process, the STING pathway can cause the occurrence of METs in renal macrophages.

3.5 The activation status of the STING pathway after exogenous mitochondrial DNA injection

Based on the previous TCE sensitization model which confirmed that STING can activate the polarization of renal macrophages and the formation of METs In order to further elaborate on the effect of liver cell mtDNA on renal macrophages we extracted the mtDNA of TCE+ mice and detected its purity and concentration using an ultraviolet spectrophotometer. A purity of 1.8-2.0 indicates good mtDNA purity, without protein or endotoxin contamination (Xie et al., 2017). The mtDNA was filtered through a 0.22um filter to remove impurities and diluted to a concentration of 25ng/μL using sterile enzyme-free PBS. We administered 5ug of purified mtDNA to the tail vein injection groups and the mtDNA + C-176 treatment

groups as per the reference literature (Zeng et al., 2024) (Fig. 5a). After the modeling was completed, we compared the differences in mtDNA content in the serum of mice from different treatment groups by detecting the double-stranded DNA content, and found that the mtDNA tail vein injection group had the highest expression of mtDNA. (Figs. 4 – 1) The ALT and AST test results of the liver function kit indicated that mtDNA tail vein injection did not cause significant abnormalities in liver function indicators, while the CRE and BUN test results of the renal function kit showed that mtDNA injection could cause a significant increase in BUN in the kidneys, but there was no significant difference in CRE. (Fig. 5b) Subsequently, we detected the liver and kidney damage conditions of the mice in different treatment groups through HE staining. The results showed that the hepatocyte size and morphology of the three groups (solvent control group, mtDNA treatment group, and C-176 treatment group) changed in a regular way, the hepatocyte cords were neatly arranged in a radial pattern, there were no necrotic cells, no inflammatory cell infiltration, and no obvious damage. The HE staining results of the kidneys showed that compared with the normal saline group, the mtDNA treatment group caused mild damage to the kidneys, manifested as vacuolation of the renal tubular epithelial cells. (Fig. 5c)

In the previous liver and kidney pathological detection, it was found that after adding the STING inhibitor C-176, the biochemical indicators of the kidneys (BUN) and the pathological detection results showed a certain degree of relief. Therefore, we speculated that this was basically consistent with the previous results of the TCE model, and STING played a role in it. Thus, we detected STING expression in the mtDNA treatment group through immunofluorescence experiments and found that it was higher than that in the PBS and C-176 treatment groups, and there was a significant co-localization with F4/80. (Figs. 4 – 2) The western blotting results showed that mtDNA tail vein injection could cause an increase in STING protein expression, and we further detected the expression of downstream phosphorylated proteins of STING, and found that there was a slight increase in p-IKK/IKK, p-IKBα/IKBα, and NF-κBp-P65/NF-κBp65 proteins. (Fig. 5d)

3.6 Exogenous mitochondrial DNA causes the occurrence of polarization in renal macrophages

After confirming that intravenous injection of mtDNA can activate the STING pathway, we analyzed the occurrence of the M1 phenotype of macrophages through protein immunoblotting and immunohistochemical experiments. The immunohistochemical results showed that the expression of iNOS in the mtDNA treatment group was significantly higher than that in the solvent control group, and the expression of iNOS was mainly located in the renal tubular interstitium. The western blotting results also indicated that the expression of iNOS in the mtDNA treatment group was significantly higher than that in the solvent control group and the inhibitor group. (Fig. 6a) Subsequently, we conducted immunofluorescence co-localization analysis of the core protein citH3 of METs and the macrophage marker F4/80. The results showed that the expression of citH3 after mtDNA treatment did not show significant changes. (Fig. 6b) In addition, the protein western blotting results for the markers of METs, citH3, MPO, and PAD4, showed that compared with the normal saline group, the expression of citH3 and

PAD4 proteins in the mtDNA intravenous treatment group slightly increased, but there was no significant statistical difference. The expression of MPO showed significant differences among the three treatments. (Fig. 6c) Moreover, the ELISA results indicated that the expression of inflammatory factors IL-6 and TNF-α after mtDNA intravenous injection increased significantly. (Fig. 6d), this indicates that injection of mtDNA can trigger an inflammatory response.

3.7 The occurrence of METs after RAW264.7 cells were treated with hepatocyte mitochondrial DNA

In the previous study on the mtDNA tail vein injection model, we reported that mtDNA could cause M1 polarization of renal macrophages and increase the levels of inflammatory factors, but did not cause obvious formation of macrophage trapping nets. Therefore, we directly extracted mtDNA from the liver cells of TCE sensitized positive mice and co-cultured it with the RAW264.7 macrophage line to further explore the effect of mtDNA on macrophage trapping nets in vitro (Fig. 7a) (Jensen et al., 2023), We further added STING inhibitors to explore the expression of downstream proteins. It was found that after liver cell mtDNA stimulation, the phosphorylation level of STING downstream protein NF-κB P65 increased, while the expression of STING could be reduced by the inhibitor. (Fig. 7b) Subsequently, we further revealed the expression of M1 polarization of macrophages in response to liver cell mtDNA stimulation through immunofluorescence and flow cytometry. The flow cytometry results showed that compared with the PBS treatment group, RAW264.7 macrophages stimulated by mtDNA could significantly promote M1 polarization. (Fig. 7c) The immunofluorescence results also indicated that after liver cell mtDNA treatment, the expression of M1 polarization marker protein CD86 in macrophages significantly increased and was mainly expressed in the cytoplasm. (Fig. 7e)

As mentioned earlier, we speculated that the concentration of liver cell mtDNA in the mtDNA tail vein animal model was not sufficient to cause the occurrence of METs. Therefore, we first conducted further in vitro experiments to determine whether liver cell mtDNA could cause the occurrence of macrophage M1 polarization through the STING pathway. Then, we wanted to further verify in vitro whether liver cell mtDNA could cause METs. We first detected the release of METs after treatment with different concentrations of liver cell mtDNA through immunofluorescence, and found that METs presented a linear blue fluorescence connected to the cell nucleus, and the macrophages showed a network and filamentous structure extension, suggesting the occurrence of METs. (Fig. 7f) In addition, the western blotting results also showed that after liver cell mtDNA treatment, the expression of METs markers citH3, MPO, and PAD4 was significantly increased (Fig. 7d). The above in vitro experimental results can reveal that liver cell mtDNA can cause macrophages to undergo M1 polarization and induce the production of METs.

Discussion

TCE sensitization is characterized by multi-organ immune injury. Some workers occupationally exposed to TCE may develop symptoms such as rash, fever, liver dysfunction, and lymphadenopathy, and this

condition is therefore referred to as OMDT (Dorsey et al., 2023). Among these manifestations, liver and kidney injuries are closely associated with disease severity and prognosis. In recent years, inter-organ communication has gradually become a new focus in the study of disease pathogenesis, and abnormal inter-organ crosstalk has been shown to be involved in the occurrence and progression of various diseases (Hur et al., 2023; Sun et al., 2023; Xia et al., 2025). However, the mechanisms by which liver injury further leads to secondary kidney injury remain unclear, which greatly hinders the diagnosis and treatment of multi-organ combined damage (Xie et al., 2024). As a central metabolic organ, the liver plays a critical role in maintaining internal homeostasis, and the “liver-kidney crosstalk” axis has attracted increasing attention (Xia et al., 2025; Yang et al., 2022). Our previous studies demonstrated that hepatocyte mtDNA, acting as a DAMP, mediates liver-kidney crosstalk during TCE sensitization, promotes M1 polarization of hepatic macrophages, and aggravates TCE-induced immune liver injury(Gao et al., 2024). However, how mtDNA regulates renal innate immune responses, particularly its interaction with macrophages, remains to be elucidated.

In the present study, we first established a TCE-sensitized mouse model and confirmed the coexistence of hepatic mitochondrial injury and renal pathological damage, accompanied by a significant positive correlation between liver and kidney function indicators. These findings suggest that hepatic mitochondrial injury may play an important role in the development of renal injury. Given the central regulatory role of macrophages in immune-related kidney injury, we further investigated the activation status of renal innate immunity. Our results showed that the cGAS-STING signaling pathway was significantly activated in the kidneys of TCE-sensitized mice, as evidenced by increased STING expression and its co-localization with the macrophage marker F4/80, along with upregulation of downstream signaling molecules. Activation of this pathway can promote NF-□B signaling and the production of inflammatory mediators, thereby creating a pro-inflammatory microenvironment that favors macrophage M1 polarization. Consistently, we observed significantly increased expression of the M1 marker iNOS, which could be effectively suppressed by the STING inhibitor C-176, indicating that STING activation is a key driver of macrophage polarization in TCE-induced renal injury. In addition to classical inflammatory responses, macrophages can release METs, which are web-like structures composed of DNA scaffolds and granular proteins. Under physiological conditions, METs contribute to pathogen clearance and immune homeostasis; however, excessive formation under pathological conditions can amplify inflammatory responses and exacerbate tissue injury. In this study, we found that METs-related markers (citH3, PAD4, and MPO) were significantly elevated in the kidneys of TCE-sensitized mice, and their expression was markedly reduced following STING inhibition, suggesting that the cGAS-STING pathway not only promotes macrophage M1 polarization but may also induce METs formation, thereby representing a novel mechanism contributing to renal inflammatory injury.

To further determine whether hepatocyte mtDNA serves as the key DAMP triggering these responses, we extracted the mtDNA from the hepatocyte of TCE-sensitized positive mice and injected it into normal mice via the tail vein. The results showed that exogenous mtDNA induced activation of the STING pathway in the kidney and promoted macrophage M1 polarization, supporting its role as a critical DAMP mediating immune activation. However, acute mtDNA exposure alone was insufficient to induce

significant METs formation or severe renal dysfunction, suggesting that this process may depend on sustained stimulation or the synergistic effects of additional inflammatory signals. In contrast, in vitro co-culture experiments demonstrated that mtDNA activated macrophages, promoted M1 polarization, and significantly induced METs formation, which could be effectively inhibited by STING blockade. These findings indicate that mtDNA has the capacity to drive macrophage activation and METs release, but its in vivo effects may depend on the intensity and duration of stimulation.

In conclusion, during TCE sensitization, hepatocyte-derived mtDNA functions as a key DAMP that activates the cGAS-STING signaling pathway in renal macrophages, thereby promoting M1 polarization and inducing METs formation, ultimately contributing to the development of renal inflammatory injury. This study expands the current understanding of liver–kidney crosstalk in TCE-induced immune injury and identifies the mtDNA-cGAS-STING-METs axis as a potential pathogenic pathway. However, several limitations remain. The precise molecular mechanisms by which mtDNA regulates METs formation require further investigation, and the potential involvement of other renal immune cells cannot be excluded. Future studies are needed to explore the therapeutic potential of targeting this pathway in TCE-related multi-organ injury.

Declarations

Author contributions

Xueqian Jia contributed to the conceptualization, methodology, investigation, formal analysis, data curation, writing – original draft;**Xuan Fan contributed to the m**ethodology, investigation, formal analysis, data curation, writing – original draft;**Chenghuan Wan contributed to the i**nvestigation, validation, data curation;**Zijun Li contributed to the i**nvestigation, formal analysis, visualization.**Luqing Pan contributed to the m**ethodology, validation, resources.**Hui Wang contributed to the r**esources, methodology, supervision,writing – review & editing;**Jiaxiang Zhang: contributed to the c**onceptualization, supervision, project administration, funding acquisition, writing – review & editing.

Funding

This work was supported by the National Natural Science Foundation of China (82273602) and the Anhui Provincial University Natural Science Research Project (2025AHGXZK20011、2025AHGXZK30177). The work was also supported by the Open Project of Key Laboratory of Dermatology (Anhui Medical University), Ministry of Education [AYPYS-2024-4]. The work was also supported by the young and middle-aged teachers training action project from Education Department of Anhui Province (JWFX2023007).

Data availability

This study did not generate or analyze any data sets.

Ethical and Legal Statement

This study was conducted in accordance with the ethical principles of the "Helsinki Declaration". The study has been approved by the Ethics Committee of Anhui Medical University, with the approval number LLSC20220971.

Publication Consent

Not applicable.

Availability of data and materials

The datasets used and/or analyzed in this study can be obtained from the corresponding author upon reasonable request.

Conflicts of Interest

The author declares that there are no conflicts of interest.

Acknowledgements

We want to thank the Platform of Environmental Exposure and Life Health Research at Anhui Medical University. We would also like to thank the“Figdraw” drawing platform for the material.

References

1. Chen, S., et al., 2023. Hepatocyte-specific Mas activation enhances lipophagy and fatty acid oxidation to protect against acetaminophen-induced hepatotoxicity in mice. J Hepatol. 78, 543–557.
2. Conceição-Silva, F., et al., 2021. The Immune System Throws Its Traps: Cells and Their Extracellular Traps in Disease and Protection. Cells. 10.
3. Dong, L. L., et al., 2025. Hepatocyte mitochondrial DNA activated store-operated Ca(2+) entry via Stim1/Orai1-induced podocyte injury in trichloroethylene sensitized mice: A new insight in liver and kidney crosstalk. Toxicol Appl Pharmacol. 503, 117465.
4. Dorsey, E. R., et al., 2023. Trichloroethylene: An Invisible Cause of Parkinson's Disease? J Parkinsons Dis. 13, 203–218.
5. Gao, L., et al., 2025. Wnt5a promotes Kupffer cell activation in trichloroethylene-induced immune liver injury. Toxicol Ind Health. 41, 83–96.
6. Gao, L., et al., 2024. Hepatocyte mitochondrial DNA mediates macrophage immune response in liver injury induced by trichloroethylene. Ecotoxicol Environ Saf. 276, 116317.
7. Garg, M., et al., 2023. Immunomodulatory role of mitochondrial DAMPs: a missing link in pathology? Febs j. 290, 4395–4418.
8. Hur, M. H., et al., 2023. Chemogenetic stimulation of the parasympathetic nervous system lowers hepatic lipid accumulation and inflammation in a nonalcoholic steatohepatitis mouse model. Life Sci. 321, 121533.

9. Jensen, M., et al., 2023. New insight into the composition of extracellular traps released by macrophages exposed to different types of inducers. Free Radic Biol Med. 202, 97–109.
10. Liu, Q., et al., 2025. Mechanisms and immune crosstalk of neutrophil extracellular traps in response to infection. mBio. 16, e0018925.
11. Ma, J., et al., 2022. Renal tubular in TCE-sensitization-induced immune kidney injury: Role of mitochondrial DNA in activating the cGAS-STING signaling pathway. Int Immunopharmacol. 113, 109432.
12. Nakajima, T., et al., 2022. Increased serum anti-CYP2E1 IgG autoantibody levels may be involved in the pathogenesis of occupational trichloroethylene hypersensitivity syndrome: a case-control study. Arch Toxicol. 96, 2785–2797.
13. Nakazawa, D., et al., 2016. The responses of macrophages in interaction with neutrophils that undergo NETosis. J Autoimmun. 67, 19–28.
14. Okubo, K., et al., 2018. Macrophage extracellular trap formation promoted by platelet activation is a key mediator of rhabdomyolysis-induced acute kidney injury. Nat Med. 24, 232–238.
15. Rasmussen, K. H., Hawkins, C. L., 2022. Role of macrophage extracellular traps in innate immunity and inflammatory disease. Biochem Soc Trans. 50, 21–32.
16. Rayner, B. S., et al., 2018. Role of hypochlorous acid (HOCl) and other inflammatory mediators in the induction of macrophage extracellular trap formation. Free Radic Biol Med. 129, 25–34.
17. Russell, D. G., et al., 2009. The macrophage marches on its phagosome: dynamic assays of phagosome function. Nat Rev Immunol. 9, 594–600.
18. Su, S., et al., 2023. Application of multiple occupational health risk assessment models in occupation health risk prediction of trichloroethylene in the electroplating and electronics industries. Int J Occup Saf Ergon. 29, 70–76.
19. Sun, J. Y., et al., 2023. An IL-6/STAT3/MR/FGF21 axis mediates heart-liver cross-talk after myocardial infarction. Sci Adv. 9, eade4110.
20. Wang, Q., et al., 2022. XBP1-mediated activation of the STING signalling pathway in macrophages contributes to liver fibrosis progression. JHEP Rep. 4, 100555.
21. Xia, L., et al., 2025. Mitochondrial DNA-activated cGAS-STING pathway in cancer: Mechanisms and therapeutic implications. Biochim Biophys Acta Rev Cancer. 1880, 189249.
22. Xian, H., et al., 2022. Oxidized DNA fragments exit mitochondria via mPTP- and VDAC-dependent channels to activate NLRP3 inflammasome and interferon signaling. Immunity. 55, 1370–1385.e8.
23. Xie, H., et al., 2024. TNF-α-downregulated SIRT1 regulates mitochondrial-autophagy and apoptosis in renal vascular endothelial cells involved in trichloroethylene-induced immune kidney injury. Int Immunopharmacol. 143, 113521.
24. Xie, L., et al., 2017. Exogenous administration of mitochondrial DNA promotes ischemia reperfusion injury via TLR9-p38 MAPK pathway. Regul Toxicol Pharmacol. 89, 148–154.

25. Yang, M., et al., 2022. Crosstalk between the liver and kidney in diabetic nephropathy. Eur J Pharmacol. 931, 175219.
26. Zeng, F. L., et al., 2024. Neutrophil extracellular traps promote acetaminophen-induced acute liver injury in mice via AIM2. Acta Pharmacol Sin. 45, 1660–1672.
27. Zuo, X., et al., 2024. Unveiling the role of mtDNA in Liver-Kidney Crosstalk: Insights from trichloroethylene hypersensitivity syndrome. Int Immunopharmacol. 138, 112513.

Figures

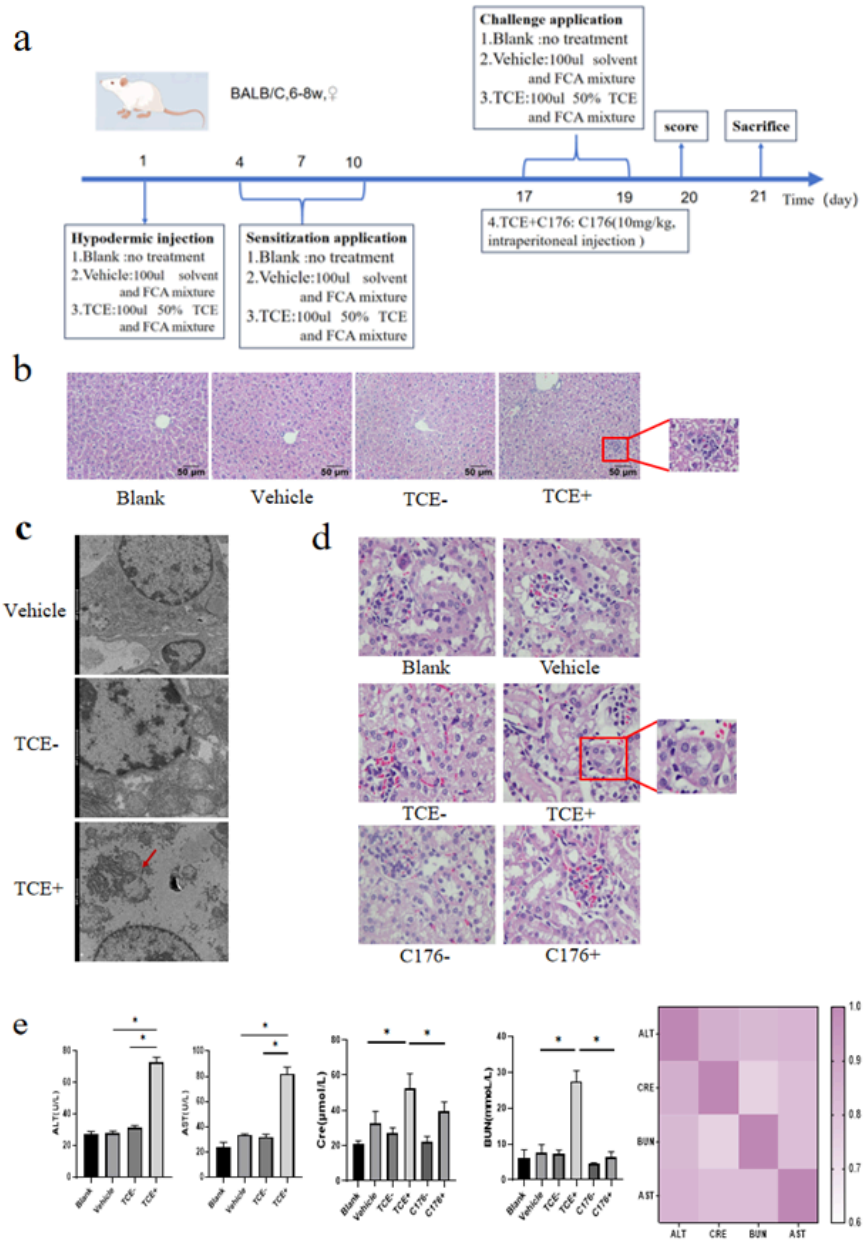


Figure 1

Mitochondrial damage in hepatocyte and kidney damage in TCE-sensitized positive mice. (a) Schematic diagram of the experimental design for establishment of the TCE-sensitized mouse model. Female BALB/c mice were used to establish the TCE-sensitized model. On the day before exposure, hair on the back was removed and the mice were numbered. On Day 0, mice received the first sensitization. On Days 4, 7, and 9, mice were topically exposed to TCE. On Days 17 and 19, mice received TCE challenge with or

without C-176 pretreatment. On Day 20, skin reactions were evaluated and biological samples were collected for further analysis. (b) H&E staining of the liver, with a scale of 50 μm. (c) Transmission electron microscopy observation of the structural changes of hepatocytemitochondria. The red arrows indicate disordered mitochondrial structure and disappearance of the outer membrane. (d) H&E staining of the kidney, with a scale of 20 μm. (e) Levels of liver function indicators ALT and AST in mouse serum, kidney function indicators CRE, BUN, and the correlation between liver function indicators and kidney function indicators. *$P < 0.05$.

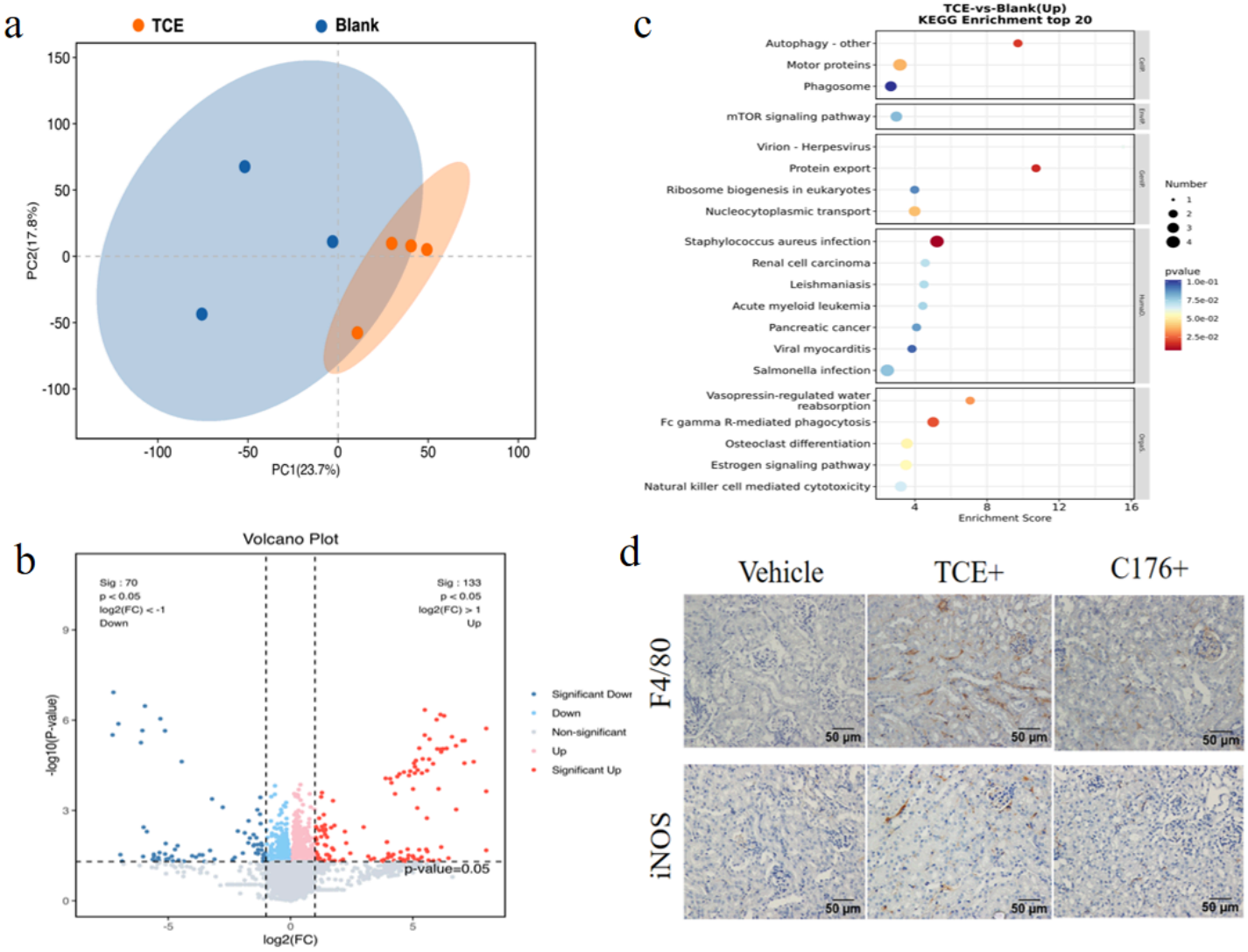


Figure 2

TCE triggers renal proteomic remodeling and macrophage inflammatory activation.(a) PCA of renal proteome shows obvious separation between TCE and blank groups, confirming divergent protein expression.(b) Volcano plot filters 203 DEPs (133 upregulated, 70 downregulated, $|\log_2 FC|>1$, $P<0.05$) in TCE kidneys vs control.(c) KEGG enrichment reveals DEPs predominantly enriched in phagocytosis and

immune-related signaling. Bubble size=enriched protein count; color=enrichment significance.(d) IHC of F4/80 and iNOS in kidney tissues: TCE elevates macrophage marker expression, while C176 reverses this increase. Scale bar=50 μm.

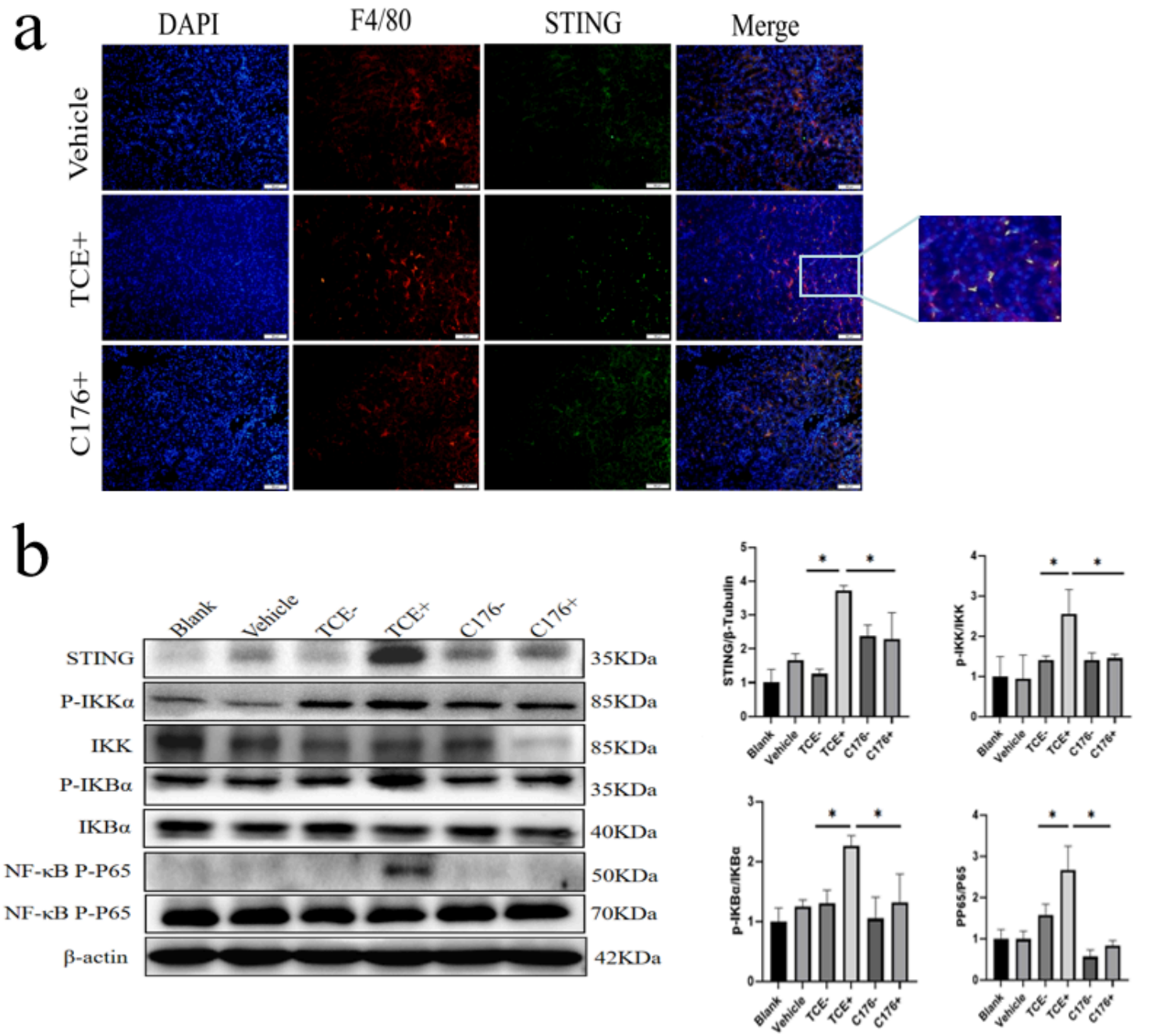


Figure 3

TCE sensitization can activate the STING pathway in renal macrophages. (a) Immunofluorescence confocal results of F4/80 and STING (×400). (b) Western blotting shows the expression levels of STING, P-IKKα/IKKα, P-IKBα/IKBα, and P-P65/P65 proteins in different treatment groups. *$P < 0.05$.

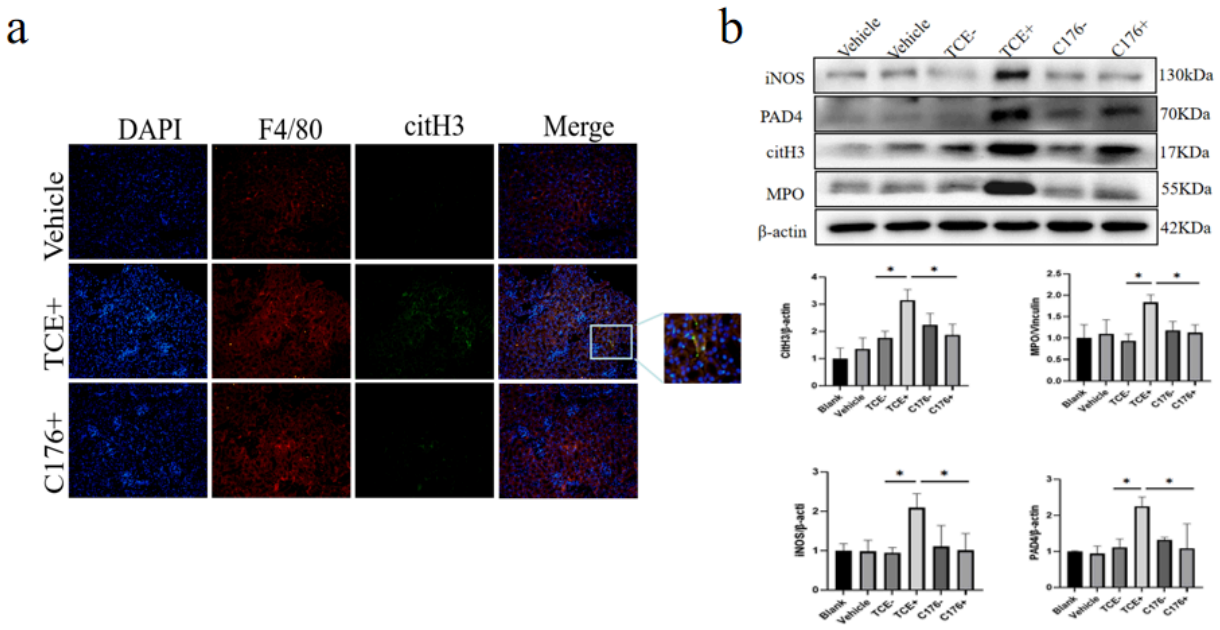


Figure 4

C176 Inhibits the Formation of TCE-Induced Kidney NETs and the Activation of M1 Macrophages.(a) Immunofluorescence shows the expression of METs marker citH3 and macrophage marker protein F4/80 in different treatment groups. (b) Western blotting shows the expression levels of polarization indicators iNOS protein and METs marker protein in different treatment groups. *$P < 0.05$.

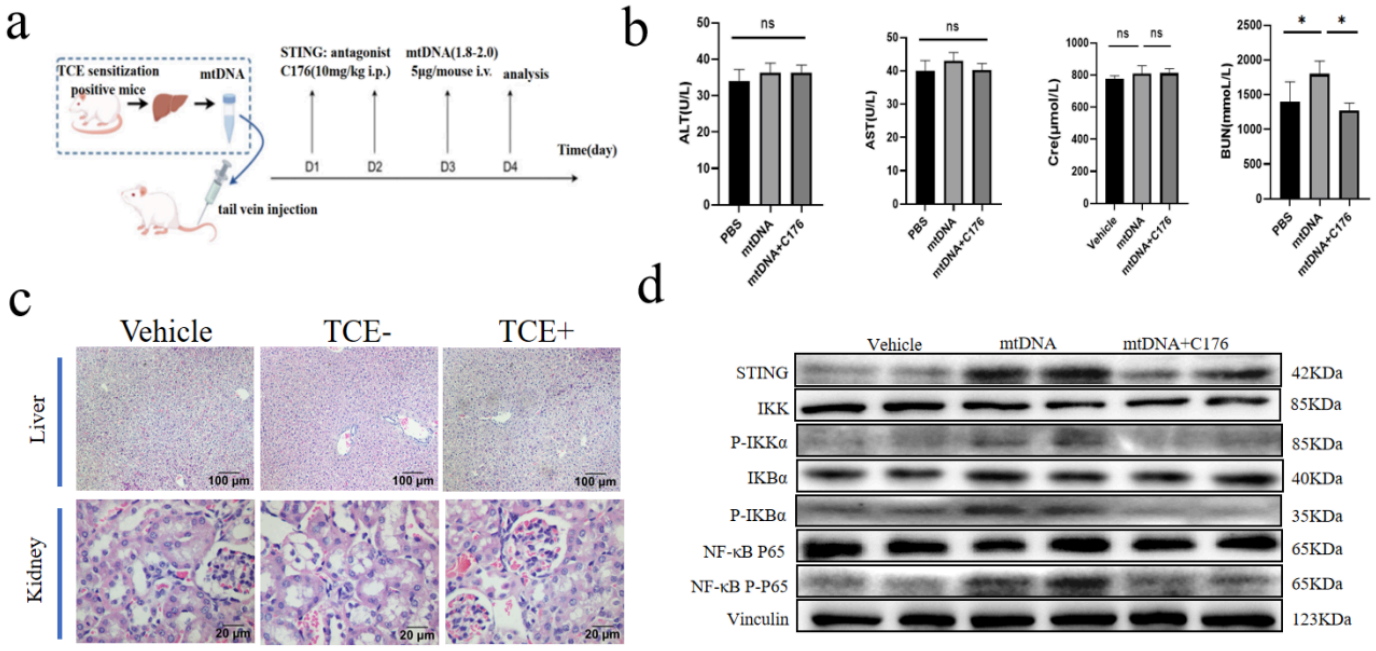


Figure 5

Injury conditions of the liver and kidneys in mice after mtDNA tail vein injection. (a) Experimental scheme for mtDNA injection and STING inhibitor treatment in mice. mtDNA was isolated from TCE-sensitized positive mice and injected into recipient mice via the tail vein, with or without C-176 pretreatment, followed by analysis. (b) Levels of liver function indicators ALT and AST in mouse serum, and levels of renal function indicators CRE and BUN. (c) H&E staining of the liver and kidney. (d) Western blotting for detecting the expression of STING and its downstream proteins. *$P < 0.05$.

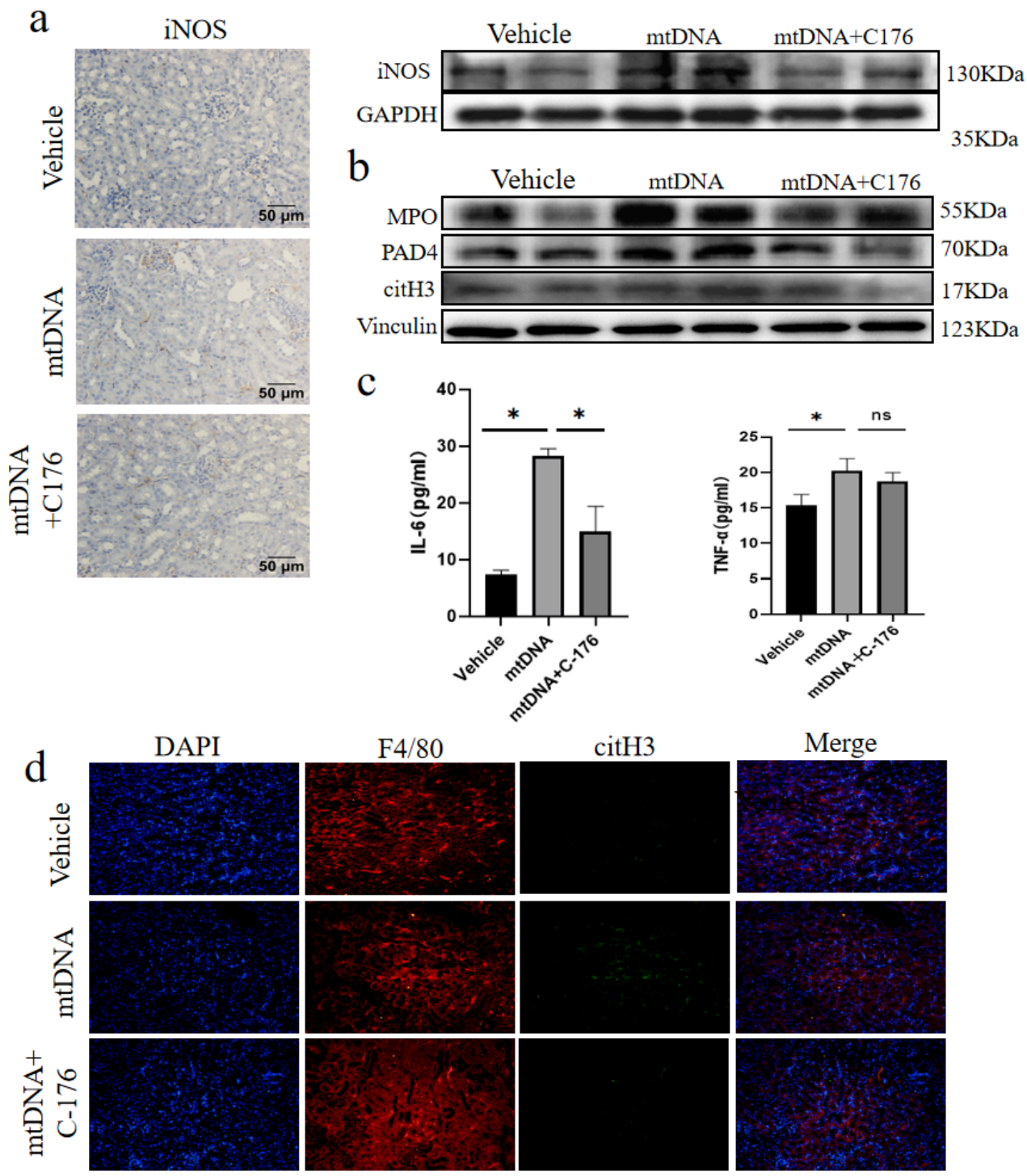


Figure 6

M1 polarization indicators, METs, and expression of inflammatory factors after mtDNA tail vein injection. (a) Immunohistochemistry shows the expression of M1 indicator iNOS in macrophages. (b) Immunofluorescence shows the expression of METs marker citH3 and macrophage marker protein F4/80 in different treatment groups. (c) Western blotting shows the expression level of METs marker

proteins. (d) Expression of inflammatory factors in mouse serum after mtDNA tail vein injection. *P < 0.05.

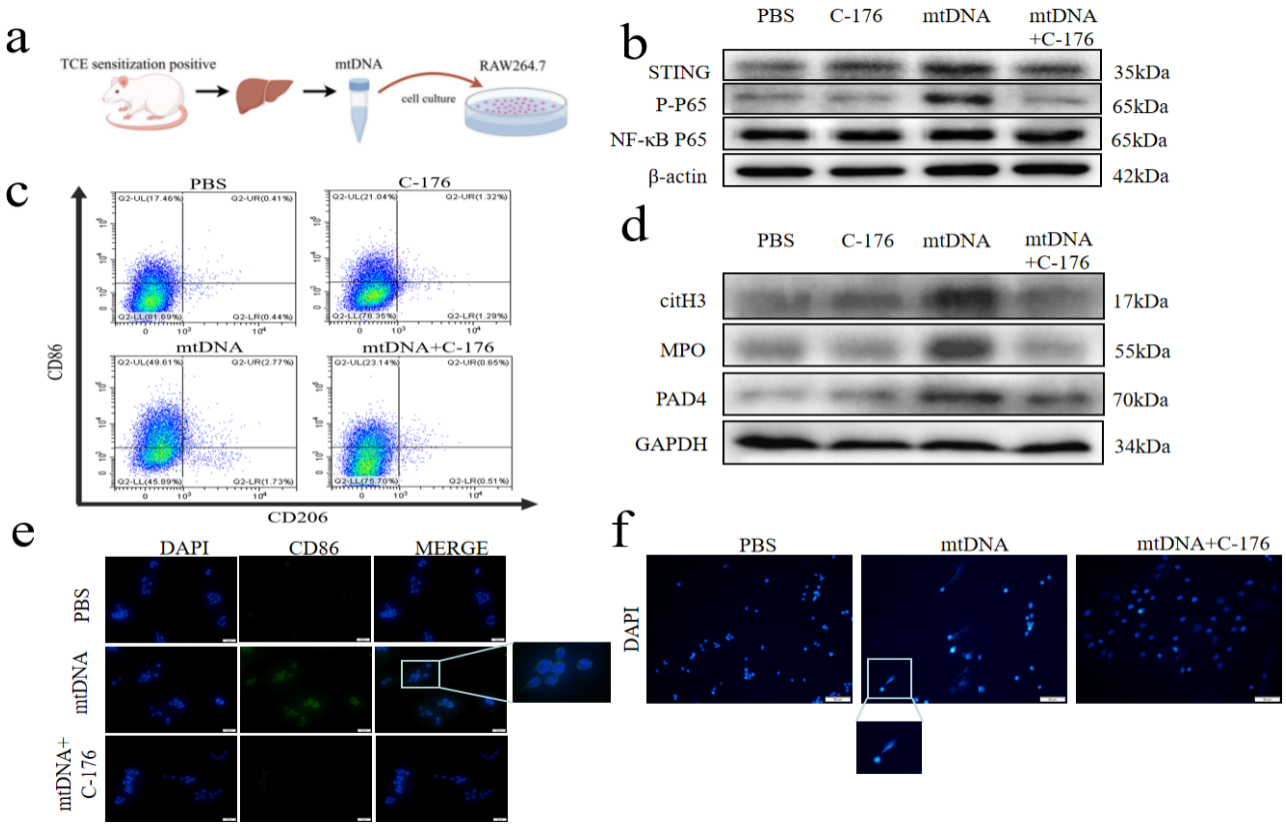


Figure 7

mtDNA co-cultured with RAW264.7 macrophages leads to M1 polarization and METs occurrence. (a) The mtDNA extracted from the livers of positive mice stimulated by trichloroethylene was used for in vitro treatment of RAW264.7 macrophages. (b) Changes in downstream proteins of STING after mtDNA treatment. (c) Flow cytometry was used to detect the expression of CD86 and CD206 on the surface of RAW264.7 cells.(d) Western blot analysis showing protein expression levels across different samples, with the bottom row serving as a loading control. *P < 0.05.(e)Expression of M1 polarization indicator CD86 after mtDNA treatment. (f) Changes in filamentous structure of cells after mtDNA stimulation of RAW264.7. Changes in METs marker proteins citH3, MPO, and PAD4 after mtDNA treatment of RAW264.7 cells.

Supplementary Files

This is a list of supplementary files associated with this preprint. Click to download.

- supplementarymaterials.docx
- floatimage1.png